Review Article
SPECT and PET imaging of adrenomedullin receptors: a promising strategy for studying pulmonary vascular diseases

Luis Michel Alonso Martinez[1,2,3], François Harel[2,3,4], Myriam Létourneau[5], Vincent Finnerty[3], Alain Fournier[5], Jocelyn Dupuis[3,6], Jean N DaSilva[1,2,4]

[1]University of Montreal Hospital Research Centre, Montréal (Québec), Canada; [2]Department of Biomedical Engineering, Faculty of Medicine, Université de Montréal, Montréal (Québec), Canada; [3]Research Center of The Montreal Heart Institute, Montréal (Québec), Canada; [4]Department of Radiology, Radio-Oncology and Nuclear Medicine, Université de Montréal, Montréal (Québec), Canada; [5]Laboratoire D'Études Moléculaires Et Pharmacologiques Des Peptides, INRS-Centre Armand-Frappier Santé Biotechnologie, Laval (Québec), Canada; [6]Department of Medicine, Université de Montréal, Montréal (Québec), Canada

Abstract: Circulating adrenomedullin (AM) levels are elevated in several cardiovascular diseases, including pulmonary vascular diseases causing pulmonary hypertension. To date the perfusion agent ^{99m}Tc-albumin macroaggregates (MAA) is the only approved radiopharmaceutical used for imaging of pulmonary circulation. Unlike ^{99m}Tc-MAA, imaging the AM receptors involves a molecular process dependent on the density of the receptors and the affinity of specific radioligands. The AM receptors are abundantly distributed in lung capillaries and its integrity provides protection in the development of pulmonary vascular diseases. This review summarizes the development and characterization of radioligands for *in vivo* imaging of AM receptors as an early predictor of the onset of a pulmonary vascular disease.

Keywords: Pulmonary arterial hypertension, pulmonary embolism, SPECT, PET, adrenomedullin radiotracers, lung microcirculation

Introduction

Adrenomedullin receptors

Adrenomedullin (AM) is a 52-amino acid peptide member of the calcitonin gene-related peptide (CGRP) family, which also includes calcitonin, two forms of calcitonin gene-related peptide (αCGRP and βCGRP), adrenomedullin-2 and amylin [1, 2]. On the one hand, CGRP mediates its effects through a heteromeric receptor composed of a G protein-coupled receptor called calcitonin receptor-like receptor (CLR) and a receptor activity-modifying protein (RAMP1) (**Figure 1A**). On the other hand, AM mediates vaso- and bronchodilating actions through specific AM receptors [3, 4]. Those are similarly composed by the heterodimer combination of CLR and RAMP2 or RAMP3, respectively, which leads to the formation of the AM

receptor subtypes 1 and 2 (termed AM1 and AM2) [5, 6] (**Figure 1B** and **1C**). The CLR component of the AM receptors belongs to the B family of the seven-transmembrane G protein-coupled receptors (GPCRs) and is conserved among the AM receptor subtypes [7]. The RAMP family comprises three members (RAMP1, RAMP2 and RAMP3) that each exhibits an N-terminal portion of 100-120 amino acids, a single transmembrane central domain, and a C-terminal segment of approximately 10 residues that is essential for glycosylation, cell-surface targeting and ligand-binding selectivity of the receptor [8].

Expression of adrenomedullin receptors

Specific AM binding sites have been identified in many tissues including the heart, blood vessels, lung and spleen [9, 10]. Particularly, AM
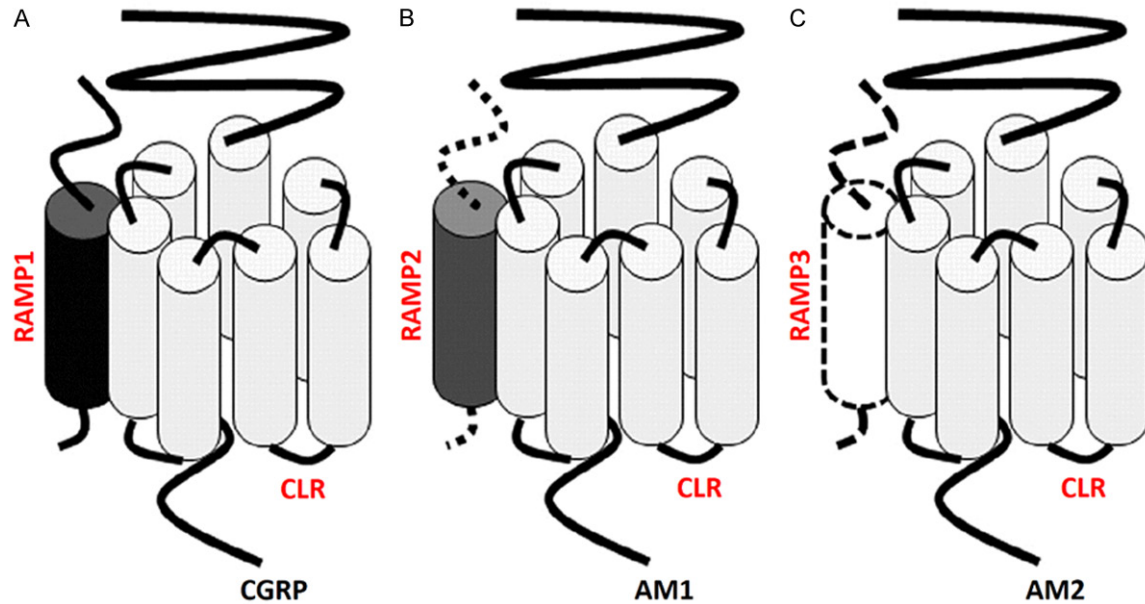
Figure 1. Composition of calcitonin gene-related peptide (CGRP) (A) and adrenomedullin receptor subtypes 1 (B) and 2 (C). Calcitonin-like receptor (CLR) is a seven transmembrane protein and the receptor activity-modifying protein (RAMP) is a component that varies in subtypes. Modified from Hay et al. [36].

receptor subtype 1 is expressed in vascular smooth muscle cells of heart, blood vessels, and spleen and its expression is markedly high in lung. Martinez et al. [11] extensively studied the expression of AM receptors in lung. Their findings suggest a specific distribution of AM and its receptors in the apical border of the epithelium and in the airway smooth muscle. AM receptors are also highly expressed in the cytoplasm of the serous cells of the bronchial glands and in type II pneumocytes, the latter being involved in the regeneration of epithelial layers of the lung. Other studies have evidenced an increased level of AM1 in the kidney and heart of rats with obstructive nephropathy and congestive heart failure [12]. In addition, a reduced expression level of RAMP2 and CLR, paired with an increase of RAMP3 levels, has been found during lipopolysaccharide-induced sepsis in rats. Also, a reduced level of the AM1 receptor components was reported in pulmonary hypertension [13-16].

Previous reports from animal models suggest that circulating AM levels are up-regulated in several cardiovascular diseases, including pulmonary vascular diseases causing pulmonary hypertension. Also, an elevation of local AM concentrations in some tumor cell lines such as carcinoids (H679, UMC11) [17], adenocarcino-

mas (H2228) [18] and to a greater extent in tumors of epithelial origin like small cell lung carcinomas H774, H123 and H735 [19, 20] was reported. Despite an association between AM and its receptor with these pathologies, the therapeutic potential of regulating the AMergic system in humans remains under-documented due to the limited information about the mechanism controlling its function [21].

Pulmonary hypertension

Pulmonary hypertension (PH) is characterized by a mean pulmonary artery pressure >20 mmHg [22] and is the result of numerous disorders that may directly or indirectly affect the integrity of pulmonary circulation. As a general consensus, this disorder is difficult to diagnose, and in most cases there is a rather large time gap between the initial clinical manifestation and the diagnosis, thereby evidencing the needs of early detection strategies of pulmonary vascular diseases [10]. This delay is in part due to the non-specific symptomatology caused by pulmonary vascular diseases, shortness of breath, and to the current diagnostic gold standard that requires invasive hemodynamic measurement of pulmonary artery pressures. Although non-invasive methods, such as cardiac ultrasound, can be utilized for screen-

ing, there is currently no biomarker for the disease, as well as no imaging method that directly assesses pulmonary vascular biology.

The integrity of pulmonary circulation is currently anatomically imaged by X-ray, chest CT angiography, MRI and pulmonary angiography with radiologic contrast [23]. Lung perfusion scanning with ^{99m}Tc-albumin macroaggregates (MAA) is the most utilized procedure to dynamically study the pulmonary vasculature. However, ^{99m}Tc-MAA has the limitation of not allowing the investigation of the pulmonary microcirculation due to their large size, thus causing their trapping in small pulmonary vessels and preventing visualization beyond the point of blockage [24]. Furthermore, being a physical tracer, ^{99m}Tc-MAA distribute solely according to the relative supply of blood flow and does not provide information on the biology of the pulmonary circulation.

At the microcirculation level, endothelial injury is an early event in the development of a pulmonary vascular disease [25]. In particular, this disorder is characterized by a dysregulation of transporters and specific receptors such as the AM receptors [10]. Thus, we hypothesized that a molecule targeting endothelial metabolic functions, like does AM, could serve as an imaging agent of pulmonary microcirculation.

SPECT adrenomedullin radioligands

Initial proof of concept: ^{125}I-rAM (1-50)

Biodistribution, pharmacokinetics and multi-organ clearance of ^{125}I-rAM (1-50) (**Figure 2A**) were evaluated in rats. After injecting the tracer (200 µL, 18.5 kBq, 0.5 µCi), blood samples were collected 1 min post-injection and then this step was repeated every 5 min for a 30-min period. The tracer exhibited a fast distribution half-life of 2 min and an elimination of 15.9 min that was not affected by the administration of hAM (22-52), CGRP or unlabeled rAM (1-50). ^{125}I-rAM (1-50) was predominately retained 20 times more efficiently in the lungs than any other organs, and the uptake was found to be specific to AM receptors after blocking with unlabeled rAM (1-50). There was also no difference in plasma and tissue levels of endogenous AM demonstrating that lungs are the primary site for clearance of ^{125}I-rAM (1-50),

mediated via a specific murine AM receptor process at the vascular endothelium level [26].

Single-pass measurement of AM clearance was performed in dogs using the single bolus indicator-dilution technique. A bolus of 122 kBq (3.3 µCi) was injected, and the samples were collected and processed to construct the indicator-dilution curves. After a baseline single bolus dilution, AM (22-52), CGRP or unlabeled rAM (1-50) was administered to perform a second indicator-dilution experiment [26]. The findings suggested an important first-pass extraction of ^{125}I-rAM (1-50) that was greatly reduced after injection of unlabeled rAM (1-50), slightly decreased after AM (22-52), and unaffected by CGRP, revealing a specific binding to AM receptors. Altogether, these experiments indicated that there is an important first-pass pulmonary clearance in the lung and that ^{125}I-rAM (1-50) binds with a very high affinity to its receptor.

*[99m]Tc-labeled DTPA-AM*

Synthesis: Disulfide bridged DTPA-human AM (1-52) is identical to native human AM, except for the addition of DTPA as a ^{99m}Tc chelator at the N terminus (**Figure 2B**) [24]. Using DTPA dianhydride, the chelating moiety was incorporated into the peptide chain and purified by reverse-phase HPLC (RP-HPLC). The conjugate was radiolabeled with ^{99m}Tc in presence of $SnCl_2$ in acidic media, at room temperature for 1 h, and then purified by RP-HPLC. The radiochemical purity was 93±2%.

In vitro evaluation: Tracer affinity was evaluated in human breast adenocarcinoma MCF-7 cells by competitive-binding experiment with ^{125}I-hAM (1-52). The IC_{50} value of DTPA-AM was calculated as 19 nM, which is within the expected range for a specific AM ligand [24].

In vivo evaluation: Plasma kinetics and biodistribution of ^{99m}Tc-DTPA-AM (18.5 µg, 185 MBq, 5 mCi) were studied in healthy dogs. Plasma levels rapidly decreased following a bi-compartmental model with a distribution half-life of less than 2 min and an elimination half-life of 42 min. In addition, the rate constant between the central and peripheral compartments was established at 24, thereby showing an important distribution into the peripheral compartment [24].
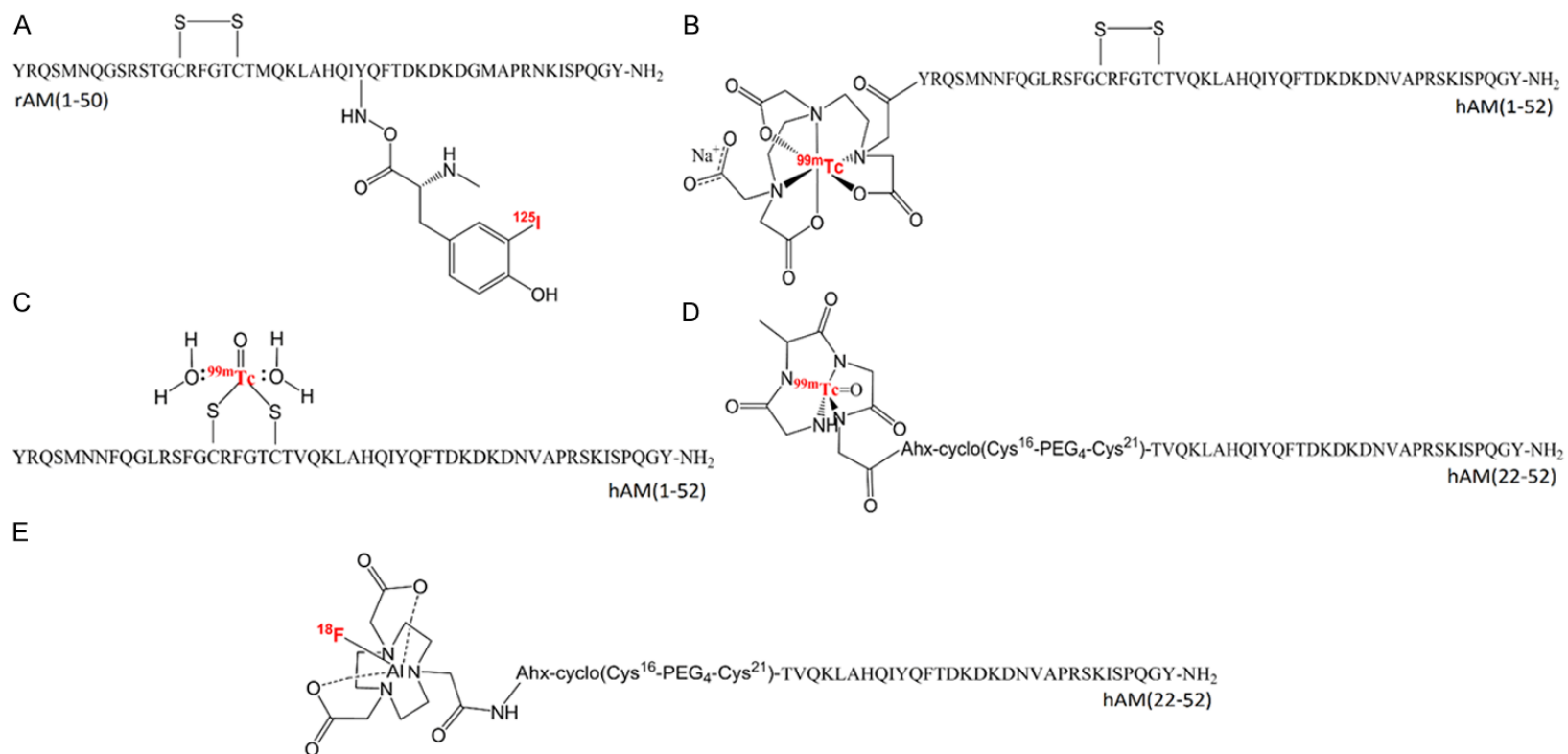
Figure 2. Adrenomedullin SPECT and PET radiotracers. Proof of concept: ^{125}I-rAM (1-50) (A) ^{99m}Tc-DTPA-AM (B) ^{99m}Tc-Cys[16,21]-AM (C) ^{99m}Tc-PulmoBind (D) and Al[18]F-DFH17 (E).

Biodistribution and multi-organ clearance were evaluated by dynamic planar and static SPECT imaging. Dynamic acquisitions of the lungs, heart, liver, and kidneys were recorded for 30 min, while static acquisitions were also recorded for whole individual organs (lungs, kidneys, liver, heart, bladder, and gallbladder) at 30, 60, and 120 min after the initial injection. The result demonstrated that the lungs predominantly retained the peptide with 27±1% of the injected dose (ID) at 30 min post-injection. The kidneys and liver also exhibited important uptakes with 19±1% ID and 12±1% ID, respectively. Tracer retained in the lung was slowly washed out over time maintaining approximately 20% of the injected dose after 120 min [24]. Hence, cyclic ^{99m}Tc-DTPA-AM derivative exhibited significant lung uptake but important retention in liver and heart were found to potentially decrease its interest as a SPECT imaging agent.

^{99m}Tc-labeled-AM through the free Cys^{16,21}-SH functions ((S-^{99m}Tc-S)-AM)

Synthesis: The linear AM derivative (L-AM), containing free SH groups on cysteines 16 and 21, was directly radiolabeled with technetium via chelation of oxotechnetium (V) with the cysteine residues, using SnCl$_2$ as a reducing agent (**Figure 2C**). Similar to the parent molecule DTPA-AM, the radiolabeling was performed in acidic media for 1 h. Moreover, a study with different linear AM fragments i.e. AM (13-52) and serial AM fragments ranging from 16-52 to 22-52 showed that only the peptides containing both cysteine residues were able to chelate ^{99m}Tc(V)O^{2+}. The labeling efficiency for linear free SH AM was 55% but with an unexpected high 35% of radiocolloids. After purification by C$_{18}$ Sep-Pak, (S-^{99m}Tc-S)-AM was produced with a radiochemical purity ≥95%. The average specific activity was 51.8±15 MBq/nmol (1.4±0.4 mCi/nmol) [24].

In vitro evaluation: Similar to that of DTPA-AM, the L-AM affinity was evaluated in human breast adenocarcinoma MCF-7 cells by competitive-binding experiment with ^{125}I-hAM (1-52). The IC$_{50}$ value was 70 nM confirming the competitive binding of the L-AM form in human cells expressing the AM receptors. Dog lung homogenates were also used to study the affinity and selectivity of L-AM, along with other agonists and antagonists of the calcitonin peptide fami-

ly, by receptor-binding assays using ^{125}I-hAM (1-52). Although it was weaker than the native molecule, the linear peptide exhibited excellent affinity and selectivity for canine AM receptor subtype 1 over those of other peptides like adrenomedullin-2 (AM2), amylin and pro-adrenomedullin N-terminal peptide [27].

In vivo evaluation: Plasma kinetics and biodistribution of the (S-^{99m}Tc-S)-AM derivative were studied in healthy dogs. The pharmacokinetic two-compartment model resulted in a distribution half-life of 1.7 min and an elimination half-life of 32 min, thus evidencing a slightly faster elimination than ^{99m}Tc-DTPA-AM. Transpulmonary indicator dilution with Evans blue dye-labeled albumin was used to precisely quantify the first-pass clearance of (S-^{99m}Tc-S)-AM. The tracer single-pass pulmonary extraction was 30±5% being almost the same as that of ^{125}I-rAM. Hence, as previously demonstrated with ^{125}I-rAM, lungs are the primary site for clearance of (S-^{99m}Tc-S)-AM mediated via AM receptors. Biodistribution and multi-organ clearance were evaluated by dynamic and static SPECT imaging as described for the cyclic ^{99m}Tc-DTPA-AM derivative. Unexpectedly, the (S-^{99m}Tc-S)-AM peptide had a higher uptake in the lungs than the cyclic derivative (42±5% vs 27±1%). Also, a lower uptake in the liver and higher levels of urinary elimination were found with the tracer derived from linear AM, making this derivative an attractive imaging agent. Moreover, a study using (S-^{99m}Tc-S)-AM in dogs, following a surgical ligation of the pulmonary arteries, demonstrated that this radioligand could be used to visualize lung perfusion defects because anatomic perfusion mimicking large pulmonary embolism was easily detectable [27].

Finally, evaluation of (S-^{99m}Tc-S)-AM in the rat monocrotaline-induced PH model, a paradigm that mimics group 1 pulmonary arterial hypertension (PAH), resulted in lower pulmonary uptake in the animals. This treatment causes progressive obliteration of pulmonary vessels that is associated with a reduced lung expression of RAMP2, the specific heterodimeric component of the AM1 receptor [15]. This finding was the first evidence of a direct correlation between the 80% decrease of RAMP2 protein expression, as measured by Western blot, and the approximate 70% reduction in lung uptake found during the SPECT imaging experiment.

Taking all this into account, the authors concluded that the novel imaging agent could potentially diagnose PAH and other similar disorders.

99mTc-PulmoBind

Structure-activity relationship (SAR) studies: SAR studies were performed to characterize the structural requirements of human AM for binding sites in dog lungs. The AM derivatives (fragments 13-52, 22-52, 26-52, 1-25, 40-52 and 1-40) were produced by Fmoc solid-phase peptide synthesis and characterized *in vitro* by displacement of ^{125}I-hAM (1-52) [28]. First, the study demonstrated that deletion of 12 or 21 N-terminal residues, to generate fragments AM (13-52) and AM (22-52), induced a significant decrease in binding affinity, whereas deletion of four extra amino acids (AM (26-52)), led to a compound unable to bind the AM receptors present in the lung. Second, the C-terminal fragment AM (40-52) produced no displacement while C-terminal deletions (fragments 1-25 and 1-40) induced dramatic losses of binding properties [27]. All these results suggested that the C-terminal portion of the peptide, in which is localized an α-helix structure, is essential for binding to AM receptors. Moreover, the study showed that a disruption of the disulfide bridge involving the cysteine residues 16 and 21 also reduced receptor affinity, demonstrating an important role for the disulfide bond, probably by stabilizing the secondary structure of the peptide. Finally, the order of potency for binding inhibition was AM>>linear AM (1-52)>AM (13-52)>AM (22-52)>AM (26-52)>AM (1-25), AM (40-52) and AM (1-40) [29].

Synthesis: Considering the SAR studies and the data obtained with (S-^{99m}Tc-S)-AM, the fragments 13-52 and 22-52 were further investigated as potential AM-based lung molecular imaging agents. The AM derivatives were synthesized in high purity (≥92%) by solid-phase and radiolabeled with ^{99m}Tc, as previously described [24, 27]. Particularly, three compounds based on AM (22-52) were modified with a 4 unit-PEG spacer, aimed at substituting the intracyclic amino acid residues promoting the AM vasodilating action, and a Gly-Gly-D-Ala-Gly N_4-type chelator. Among these AM derivatives, the disulfide bridged fragment Gly-Gly-D-Ala-Gly-Cys^{16}-(PEG)$_4$-Cys^{21}-hAM (22-52) called

PulmoBind was synthesized with 97% chemical purity (**Figure 2D**). PulmoBind and the other analogues were radiolabeled with Sn^{2+}-reduced technetium-99m, in a buffered solution (pH 4.5) at room temperature for 15 min. Labeling efficiencies were determined by iTLC-SG. The tracers were purified via a C$_{18}$ Sep-Pak and reformulated in PBS pH 7.4. As expected, the ^{99m}Tc direct labeling of AM derivatives resulted in lower radiochemical yields (65%) compared to chelator-modified AM derivatives (≥80%). Among all compounds, ^{99m}Tc-Pulmo-Bind exhibited the greatest capacity to stably complex ^{99m}Tc [29].

In vitro evaluation: The binding ability of PulmoBind was evaluated in dog lung homogenates by saturation and competitive displacement experiments with ^{125}I-hAM (1-52). Saturation studies demonstrated that ^{99m}Tc-Pulmo-Bind was bound to specific binding sites with a density of 2,317±320 fmol/mg and affinity of Kd=2.6±0.8 nM. In contrast, (S-^{99m}Tc-S)-AM resulted in a receptor density of 1,222±148 fmol/mg and a Kd of 0.17±0.07 nM suggesting that PulmoBind could occupy more binding sites than AM but with lower affinity. Surprisingly, ^{125}I-hAM (1-52) and PulmoBind displacement curves were statistically indistinguishable, suggesting that AM and PulmoBind competed for the same binding site in dog lungs [30].

In vivo evaluation: ^{99m}Tc-PulmoBind as well as other AM derivatives were evaluated in mongrel dogs (**Figure 3B**). The radioligands (185 MBq, 5 mCi) were injected intravenously via the jugular vein and whole-body biodistribution was evaluated by a dual head gamma-camera (Siemens) equipped with a low-energy parallel-hole collimator. Dynamic acquisitions were recorded for a 30-min period, and static whole-body scans were obtained at 30, 60, and 120 min at a scan speed of 10 cm/min. Among all derivatives, at the first min post-injection, ^{99m}Tc-Pulmobind had a lung first pass comparable to AM (~75% ID), which was then reduced to 40% in an uptake plateau that was maintained up to 1 h. At later points, uptake in kidneys and bladder was higher than in other tissues with concomitant decreases in lung, heart, and liver, indicating that PulmoBind was eliminated mainly through renal excretion [29].

Additionally, since native AM is primarily a vasodilator with hypotensive effects, the hemody-
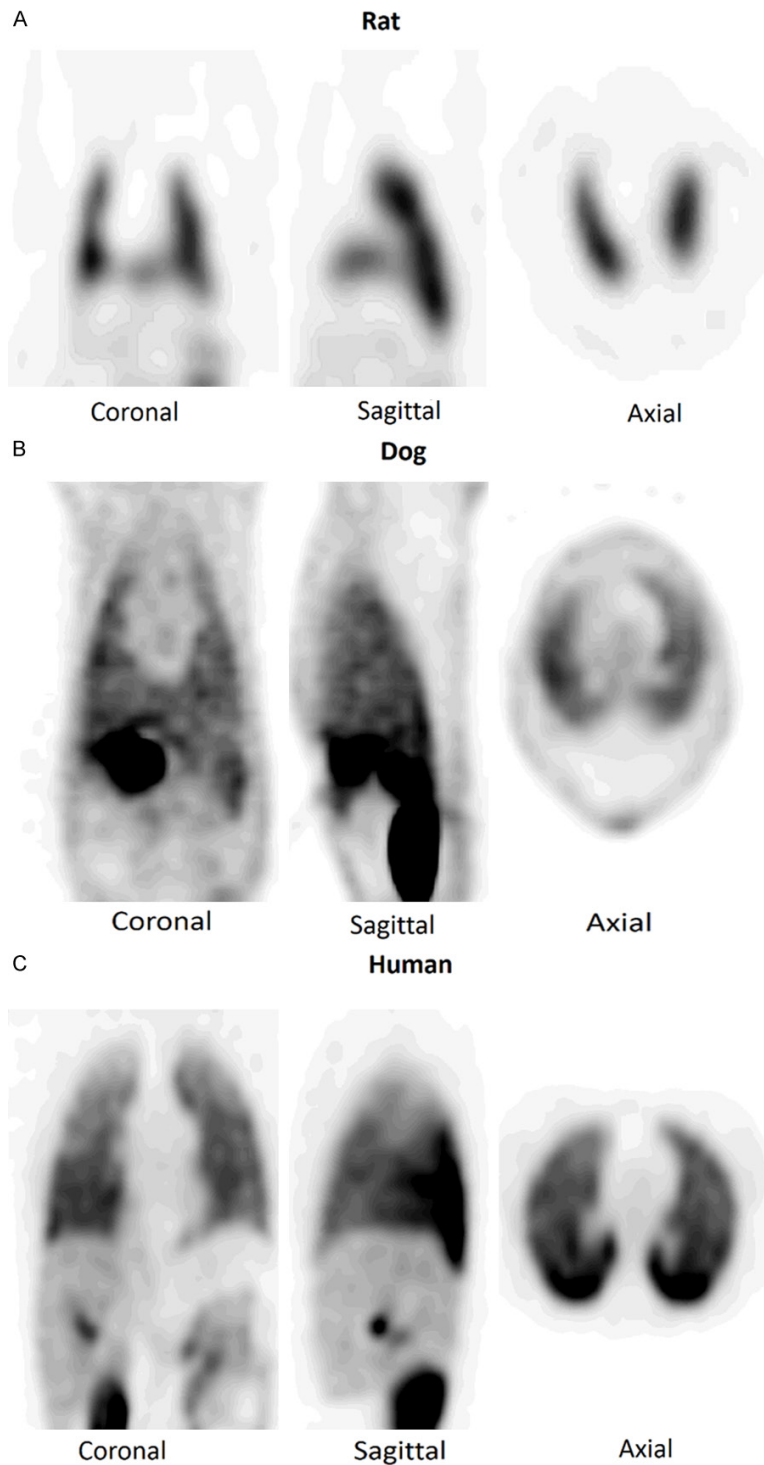
Figure 3. Whole body images of ^{99m}Tc-PulmoBind activity (30-75 min post-injection) in Sprague-Dawley rat (A), mongrel dog (B) and human (C).

nous injections, native human AM clearly dropped the mean arterial blood pressure (MAP), an activity that was accompanied with an elevation in heart rate. In contrast, PulmoBind did not produce significant variations in MAP and heart rate up to a dose close to 100X the estimated lung scan dose. In addition, PulmoBind injection did not cause any significant hemodynamic effects at 300X the estimated lung scan dose in rats.

These results demonstrated that the 17 to 20 segment of AM (Arg^{17}-Phe^{18}-Gly^{19}-Thr^{20}) plays a crucial role in the vasodilating effect of this peptide and that receptor affinity is mostly associated with the C-terminal portion of the molecule. Hence, the substitution of the intracyclic amino acids with a PEG$_4$ spacer was an efficacious strategy to maintain a good affinity while reducing potently the hypotensive effects. Moreover, the conservation of the cyclic structure by keeping the disulfide bridged cysteine residues at position 16 and 21 is also a key feature of the ligand, as shown with the mixed results obtained with the linear analogue in which the Cys side chains were capped with acetamidomethyl (Acm) groups, in order to maintain the peptide linearity. Accordingly, the cyclic Cys^{16}-PEG$_4$-Cys^{21} structure, mimicking in size and constraint the cyclic core shaped in AM by the Cys^{16}-Arg^{17}-Phe^{18}-Gly^{19}-Thr^{20}-Cys^{21} segment, appears to stabilize the molecular geometry of the C-terminal stretch of the peptide and favors binding by facilitating its interaction with the AM1 receptor.

namic effect of PulmoBind and other AM analogues were evaluated in dogs by means of pulmonary artery pressure monitoring with a Swan-Ganz catheter. After cumulative intrave-

99mTc-PulmoBind was further evaluated in the monocrotaline-induced PAH model, as previously described above. Rats were anesthetized for hemodynamic measurements and SPECT scans. *In vivo* biodistribution revealed a markedly reduced lung uptake of PulmoBind, from 12±2% ID in control rats to 4±1%, in rats with pulmonary arterial hypertension [29]. This result clearly demonstrated that 99mTc-PulmoBind was able to detect lung microcirculatory perfusion defects associated with PAH, without causing any adverse hemodynamic responses.

Human studies: The safety, efficacy and dosing of PulmoBind was evaluated in a clinical trial phase I (NCT01539889) for molecular imaging of pulmonary circulation (**Figure 3C**) [31]. Healthy individuals (n=20) were included into dose-scaling groups of 99mTc-PulmoBind: 185 MBq (5 mCi, n=5), 370 MBq (10 mCi, n=5), or 555 MBq (15 mCi, n=10). Specific activity was estimated to be around 252 MBq/mmol (6.8 mCi/mmol). Afterward, SPECT imaging and dosimetry were serially performed. The study revealed no safety concerns at the three dosages studied. Image analysis displayed a predominant and prolonged tracer uptake in lung with a mean peak extraction of 58±7%. 99mTc-PulmoBind was generally well tolerated, with no clinically-significant adverse event related to the product since no changes in systolic and diastolic pressure, respiratory rate, oxygen saturation and body temperature were detected. At the highest dose of 555 MBq (15 mCi) the tracer provided excellent images with favorable dosimetry (effective dose of approximately 6 to 8 mSv). At a dose of 555 MBq, nuclear medicine specialists judged the quality of imaging obtained with PulmoBind as superior to that attained with MAA. The study concluded that 99mTc-PulmoBind is safe and provides good quality lung perfusion imaging [31], and that the dose of 555 MBq can be used for further developments.

Subsequently, the safety of 99mTc-PulmoBind and its capacity to detect pulmonary vascular diseases associated with PH was evaluated in a human phase II study (NCT02216279) [30]. Thirty patients with PAH (group I PH, N=23) or chronic thromboembolic PH (CTEPH, group IV PH, N=7) with WHO functional class II (N=26) or III (N=4) were compared to 15 healthy subjects (control group). 99mTc-PulmoBind was adminis-

tered at the previously established dose of 555 MBq (340±42 MBq/nmol, 9.18±1.14 mCi/nmol,) and SPECT/CT images were acquired in supine position after 35 min. Dynamic planar images were obtained for the first 35 min and static images after 60 min. Qualitative and semi-quantitative analyses of lung uptake were performed and the analysis found a markedly abnormal pattern in the PH group. In fact, approximately 50% of subjects presented abnormalities ranging from moderate to severe in heterogeneity and extent. The abnormalities were unevenly distributed between the right and left lungs as well as within each lung. Compared to controls, segmental defects compatible with pulmonary embolism were present in 7 out of 7 subjects with CTEPH and in 2 out of 23 subjects with PAH. Additionally, 99mTc-PulmoBind activity distribution index was elevated by 59% in PAH compared to controls, evidencing the degree of severity of PAH group. 99mTc-PulmoBind lung SPECT was completely normal for the only individual included in the study with vasodilator-responsive idiopathic PAH, a rare form of group I PH with excellent prognosis and responsive to therapy. Repeated testing in healthy controls after one month was well tolerated and showed no significant variability of 99mTc-PulmoBind distribution. Taking all this into account, 99mTc-PulmoBind SPECT imaging of the pulmonary vascular endothelium was found to be safe in PH and showed potential to detect both pulmonary embolism and abnormalities indicative of PAH. To this extent, a PulmoBind Phase III study is now required to directly compare with other perfusion agents such as labeled macro-aggregates of albumin and angio-CT, and determine its capacity to detect pulmonary vascular diseases at earlier stages than is currently clinically available.

PET radioligands for adrenomedullin receptors

A radiofluorinated AM derivative was recently developed for PET imaging of pulmonary microcirculation offering key advantages such as higher resolution images and more sensitive uptake, facilitating the quantification of AM receptors with potentially less false positives.

Al[18]F-DFH17

Synthesis: Based on PulmoBind, the human AM derivative DFH17 (**Figure 2E**) was produced by Fmoc solid-phase peptide synthesis using the

same pegylated core Cys^{16}-$(PEG)_4$-Cys^{21} [32]. The pegylated peptide was then coupled to an aminohexanoyl spacer and derivatized with the macrocyclic chelator NOTA for radiometal complexation chemistry. DFH17 was produced in 94% chemical purity and was radiofluorinated using the $Al^{18}F$ method [33]. Complexation studies with maleimido-NOTA were initially performed to find the optimal reaction conditions. Then, DFH17 was successfully radiolabeled with $Al^{18}F$ at a 22-38% (n=6) radiochemical yield and with a 99% radiochemical purity [32].

In vivo evaluation: $Al^{18}F$-DFH17 was in *vivo* evaluated in Sprague-Dawley rats, mongrel dogs and rhesus monkeys (**Figure 4**). CT images and Dynamic PET were acquired on a PET-CT clinical imaging system (Siemens Biograph mCT Flow 40, Germany). Rats were injected with $Al^{18}F$-DFH17 (~74 MBq, 2 mCi, 0.3 mL) and whole-body PET images were acquired (6×10 min frames), 15 min after radiopharmaceutical injection [32]. A mongrel dog was injected intravenously with 296 MBq (8 mCi, 8 mL) via the jugular vein through a 3-way stopcock 18-French catheter for lung uptake evaluation. Whole-body PET images were acquired (6×10 min frames), 15 min after radiopharmaceutical injection. Dynamic PET image centered on the lungs were acquired over a period of 15 minutes and then 8 whole-body PET images were obtained up to 90 min after radiopharmaceutical injection. A non-human primate whole-body PET imaging was performed delineating the liver, kidneys, testes, lung, and a gut region as regions of interest. Dosimetry estimations were obtained with the OLINDA-Organ Level Internal Dose Assessment software package. A conservative bladder voiding time of 4.8 h was assumed to obtain the estimates.

Compared to the control animal, high tracer accumulation was observed in rat lungs 5 min post-injection and persisted for 1 h (3% ID). The tracer was rapidly excreted by the kidneys and biodistribution in other non-target organs were considerably low (**Figure 4A**). The tracer also exhibited high *in vivo* stability since no radioactivity was observed in the bones even at 1 h post injection. A similar profile was found in the dog and primate with a rapid $Al^{18}F$-DFH17 accumulation in lungs after 5 min post-injection (**Figure 4B**) and that remained up to 200 min (rhesus monkey) with a clear elimination pathway via the urinary system (**Figure 4C**).

Particularly in the monkey, the uptake in the right lung was greater than the left lung presumably due to differences in perfusion between the two lungs. Signs of *in vivo* stability were found in all species since uptake in the bones due to de-fluorination of $Al^{18}F$-DFH17 was not observed (**Figure 4**).

Time-activity curves (**Figure 4**) display that lung uptake is species-dependent with an increasing uptake of $Al^{18}F$-DFH17 from rat to monkey. Analysis of the human and mouse transcriptomes revealed that the RAMP2 component of AM1 was relatively equally distributed among most tissues with high expression levels in lung [34]. As previously reported, modifications in RAMP2 implies an uptake reduction of AM in lung [15]. Hence, using bioinformatics tools, the alignment of AM receptor sequences of various species was carried out and the data showed differences in the RAMP2 subcomponent of the receptor. As a matter of fact, only small differences in CLR sequences (primary sequence identity of 91% vs 99%) are observed, whereas high disparities are displayed when comparing RAMP2 of rat and primate (68% vs 94%). Therefore, it is believed that this large inter-species variation found in RAMP2 would be responsible for the contrasting inter-species uptake detected by PET imaging.

Calculations of absorbed radiation doses in the monkey identified the urinary bladder wall as the critical organ with an average absorbed radiation dose of 0.92 mSv/MBq. Based on the CFR 21 361.1 [35] recommendations, a maximum of 54 MBq of $Al^{18}F$-DFH17 can be administered in a single dose. In addition, the effective dose (ED) in an adult male was estimated to be 66.5 µSv/MBq (ED for F18-fluorodeoxyglucose (FDG) is ~19 µSv/MBq). Taking this value into account, a maximum of 150 MBq of $Al^{18}F$-DFH-17 can be administered within one year.

In summary, using PET imaging of AM receptors, the *in vivo* evaluation of $Al^{18}F$-DFH17 has found inter-species differences in lung uptake. These dissimilarities are attributed to differences in the RAMP2 subcomponent sequences of the AM receptor subtype 1. Considering high lung uptake, *in vivo* stability and favorable dosimetry observed in monkey, the novel AM derivative $Al^{18}F$-DFH17 exhibits an excellent
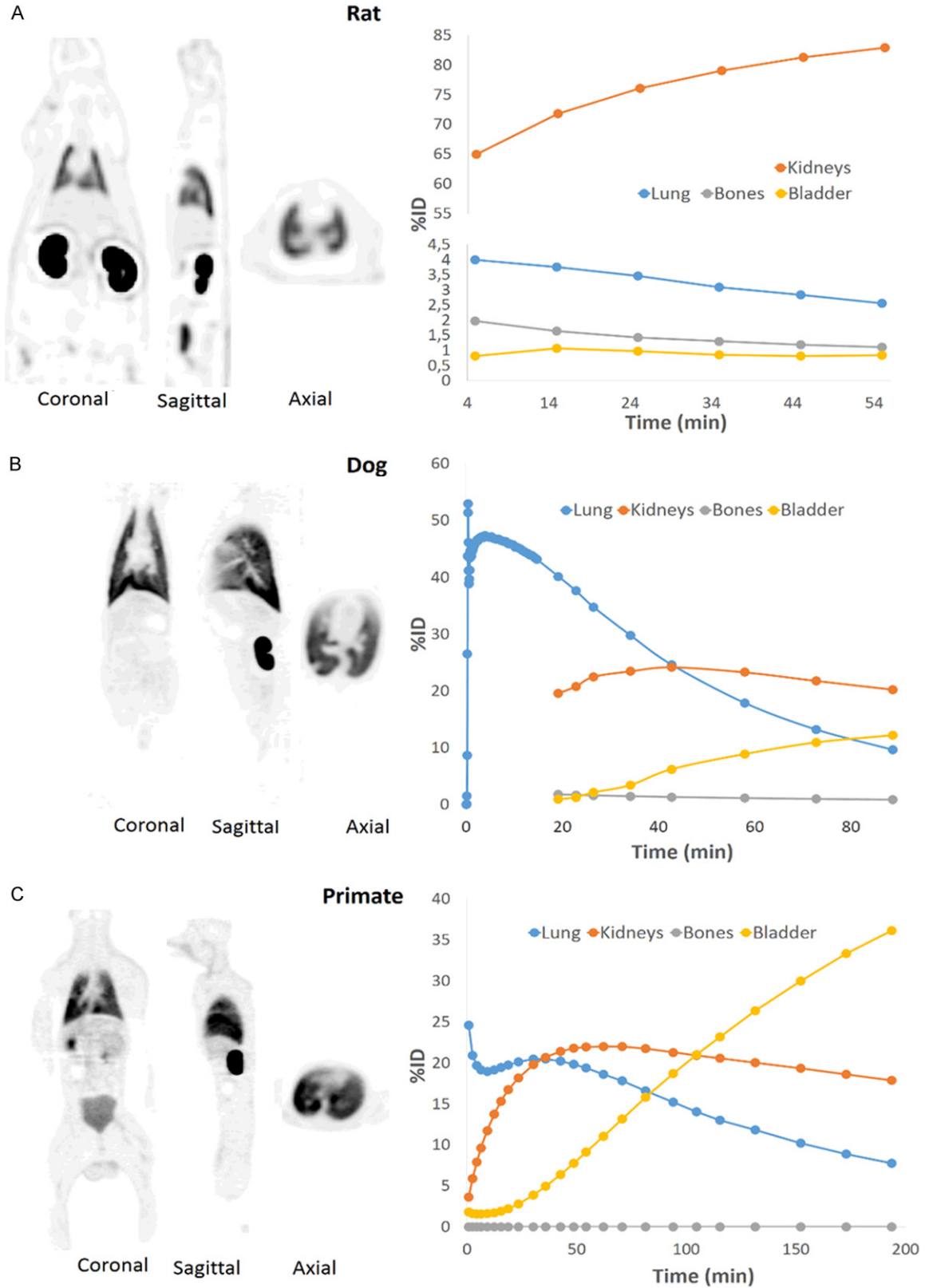
Figure 4. Whole body images of tracer activity (30-40 min post-injection, left panels) and time-activity curves (TAC, right panels) of $AI^{18}F$-DFH17 in Sprague-Dawley rat (A), mongrel dog (B) and rhesus monkey (C).

Table 1. Radiotracers for Molecular imaging of AM receptors

Modality	Radioligand	Advantages	Disadvantages
SPECT	^{99m}Tc-DTPA-AM	Rapid accumulation in lungs and renal elimination	Important retention in liver and heart
	^{99m}Tc-Cys^{16,21}-AM	High specific binding in lungs Visualization of lung perfusion defects	Low radiochemical yield, high level of radiocolloids
	^{99m}Tc-PulmoBind	High radiochemical yield and purity High target to background, favorable dosimetry Absence of hypotensive and hemodynamic effects	Attenuation-associated accuracy limit
PET	Al^{18}F-DFH17	High sensitivity, good resolution Possible quantification of AM receptors	Lower Complexation yield

potential as a PET tracer of human AM receptors.

Future perspectives

As discussed, the use of several radiotracers has proven to be a promising strategy for studying pulmonary vascular diseases via SPECT and PET imaging.

DTPA-conjugated AM opened the doors to applications of AM derivatives to image the integrity of pulmonary microcirculation. Using the well-established DTPA coordination chemistry with ^{99m}Tc, the compound was radiolabeled with more than 80% complexation yield with lower amounts of radiocolloids. This radiopharmaceutical exhibited high accumulation in the lungs with an important kidney elimination, but unfortunately its potential use was limited due to high accumulation in non-target organs such as liver and heart. The ^{99m}Tc direct labeling with a linear form of AM was then evaluated. ^{99m}Tc-Cys^{16,21}-AM was shown to bind to lung AM receptors with high affinity allowing detection of lung perfusion defects at microcirculation level. In contrast, the real applicability of this tracer was limited due to its low radiochemical yield and higher amount of radiocolloids making its synthesis process costly and inefficient (**Table 1**).

After extensive SAR studies, the tracer ^{99m}Tc-Pulmobind was designed to overcome the problems found in the past with ^{99m}Tc-DTPA-AM and ^{99m}Tc-Cys^{16,21}-AM. The compound was robustly produced in high radiochemical yield and purity using the technetium-99m one-step lyophilized kit-like approach. From animal studies to the most recent clinical trials, ^{99m}Tc-PulmoBind exhibited high target to background signal and favorable dosimetry without any serious side effect (**Table 1**). The novel tracer, Al^{18}F-DFH17, displaying high sensitivity and good spatial resolution with PET imaging was developed and evaluated in different species. Even though the complexation yield to produce Al^{18}F-DFH17 was modest, our purification approach produced this tracer in high purity allowing lung imaging in animals using PET.

^{99m}Tc-PulmoBind is thus an alternative to ^{99m}Tc-MAA for SPECT imaging of PH. Similarly, Al^{18}F-DFH17 has a great potential for studying PH with PET imaging. We believe that these two tracers will contribute to the understanding of PH related to early endothelium injury and AM receptors and, thus help to better guide PH therapy.

Conclusion

Evidences of the association between AM receptors and the development of pulmonary vascular diseases were presented along this review. In conditions leading to PH, assessment of pulmonary vascular diseases through *in vivo* quantification of AM receptors shows the capacity of evaluating endothelial injuries as an early predictor of disease and a marker of severity. Several AM tracers have been characterized for SPECT/PET imaging of pulmonary circulation. ^{99m}Tc-PulmoBind and Al^{18}F-DFH17 exhibited binding selectivity to lung AM receptors, high target-to-background ratios and a favorable dosimetry. Therefore, these radiopharmaceuticals are promising agents for future applications in molecular SPECT and PET imaging of pulmonary vascular diseases.

Acknowledgements

Disclosure of conflict of interest

J. Dupuis is administrator and shareholder of Pulmoscience inc.

Abbreviations

AM, Adrenomedullin; CGRP, Calcitonin gene-related peptide; CLR, Calcitonin receptor-like receptor; RAMP, Receptor activity-modifying protein; GPCR, G protein-coupled receptors; SPECT, Single-photon emission computerized tomography; PET, Positron emission tomography; PH, Pulmonary hypertension; MRI, Magnetic resonance imaging; MAA, Albumin macro-aggregates; rAM (1-50), Rat adrenomedullin; hAM (22-52), Human adrenomedullin fragment 22-52; DTPA, Diethylenetriaminepentaacetic acid; hAM (1-52), Human adrenomedullin; MAP, Mean arterial blood pressure; PAH, Pulmonary arterial hypertension; ID, Injected dose; CTEPH, Chronic thromboembolic pulmonary hypertension; ED, Effective dose; TAC, Time-activity curve.

Address correspondence to: Dr. Jean N DaSilva, Laboratory of Radiochemistry and Cyclotron, University of Montreal Hospital Research Centre, 900 Rue Saint-Denis, R11.440, Montréal (Québec) H2X 0A9, Canada. Tel: 514-890-8000 (30653); Fax: 514-412-7941; E-mail: jean.dasilva@umontreal.ca

References

[1] Hinson JP, Kapas S and Smith DM. Adrenomedullin, a multifunctional regulatory peptide. Endocr Rev 2000; 21: 138-167.

[2] Smith DM, Coppock HA, Withers DJ, Owji AA, Hay DL, Choksi TP, Chakravarty P, Legon S and Poyner DR. Adrenomedullin: receptor and signal transduction. Biochem Soc Trans 2002; 30: 432-437.

[3] Vachiery JL and Gaine S. Challenges in the diagnosis and treatment of pulmonary arterial hypertension. Eur Respir Rev 2012; 21: 313-320.

[4] Nuki C, Kawasaki H, Kitamura K, Takenaga M, Kangawa K, Eto T and Wada A. Vasodilator effect of adrenomedullin and calcitonin gene-related peptide receptors in rat mesenteric vascular beds. Biochem Biophys Res Commun 1993; 196: 245-251.

[5] Hay DL and Pioszak AA. Receptor activity-modifying proteins (RAMPs): new insights and roles. Annu Rev Pharmacol Toxicol 2016; 56: 469-487.

[6] Hay DL, Garelja ML, Poyner DR and Walker CS. Update on the pharmacology of calcitonin/CGRP family of peptides: IUPHAR review 25. Br J Pharmacol 2018; 175: 3-17.

[7] Conner AC, Simms J, Hay DL, Mahmoud K, Howitt SG, Wheatley M and Poyner DR. Heterodimers and family-B GPCRs: RAMPs, CGRP and adrenomedullin. Biochem Soc Trans 2004; 32: 843-846.

[8] Hagner S, Stahl U, Knoblauch B, McGregor GP and Lang RE. Calcitonin receptor-like receptor: identification and distribution in human peripheral tissues. Cell Tissue Res 2002; 310: 41-50.

[9] Yanagawa B and Nagaya N. Adrenomedullin: molecular mechanisms and its role in cardiac disease. Amino Acids 2007; 32: 157-164.

[10] Dupuis J, Harel F and Nguyen QT. Molecular imaging of the pulmonary circulation in health and disease. Clin Transl Imaging 2014; 2: 415-426.

[11] Martinez A, Miller MJ, Unsworth EJ, Siegfried JM and Cuttitta F. Expression of adrenomedullin in normal human lung and in pulmonary tumors. Endocrinology 1995; 136: 4099-4105.

[12] Muff R, Born W and Fischer JA. Calcitonin, calcitonin gene-related peptide, adrenomedullin and amylin: homologous peptides, separate receptors and overlapping biological actions. Eur J Endocrinol 1995; 133: 17-20.

[13] Nikitenko LL, Blucher N, Fox SB, Bicknell R, Smith DM and Rees MC. Adrenomedullin and CGRP interact with endogenous calcitonin-receptor-like receptor in endothelial cells and induce its desensitisation by different mechanisms. J Cell Sci 2006; 119: 910-922.

[14] Nowak W, Parameswaran N, Hall CS, Aiyar N, Sparks HV and Spielman WS. Novel regulation of adrenomedullin receptor by PDGF: role of receptor activity modifying protein-3. Am J Physiol Cell Physiol 2002; 282: C1322-1331.

[15] Dupuis J, Harel F, Fu Y, Nguyen QT, Letourneau M, Prefontaine A and Fournier A. Molecular imaging of monocrotaline-induced pulmonary vascular disease with radiolabeled linear adrenomedullin. J Nucl Med 2009; 50: 1110-1115.

[16] Merabet N, Nsaibia MJ, Nguyen QT, Shi YF, Letourneau M, Fournier A, Tardif JC, Harel F and Dupuis J. PulmoBind imaging measures reduction of vascular adrenomedullin receptor activity with lack of effect of sildenafil in pulmonary hypertension. Sci Rep 2019; 9: 6609.

[17] Sugo S, Minamino N, Shoji H, Kangawa K, Kitamura K, Eto T and Matsuo H. Production and secretion of adrenomedullin from vascular smooth muscle cells: augmented production by tumor necrosis factor-alpha. Biochem Biophys Res Commun 1994; 203: 719-726.

[18] Born W, Muff R and Fischer JA. Functional interaction of G protein-coupled receptors of the

adrenomedullin peptide family with accessory receptor-activity-modifying proteins (RAMP). Microsc Res Tech 2002; 57: 14-22.

[19] Cuttitta F, Fedorko J, Gu JA, Lebacq-Verheyden AM, Linnoila RI and Battey JF. Gastrin-releasing peptide gene-associated peptides are expressed in normal human fetal lung and small cell lung cancer: a novel peptide family found in man. J Clin Endocrinol Metab 1988; 67: 576-583.

[20] Martinez A, Elsasser TH, Muro-Cacho C, Moody TW, Miller MJ, Macri CJ and Cuttitta F. Expression of adrenomedullin and its receptor in normal and malignant human skin: a potential pluripotent role in the integument. Endocrinology 1997; 138: 5597-5604.

[21] Gibbons C, Dackor R, Dunworth W, Fritz-Six K and Caron KM. Receptor activity-modifying proteins: RAMPing up adrenomedullin signaling. Mol Endocrinol 2007; 21: 783-796.

[22] Simonneau G, Montani D, Celermajer DS, Denton CP, Gatzoulis MA, Krowka M, Williams PG and Souza R. Haemodynamic definitions and updated clinical classification of pulmonary hypertension. Eur Respir J 2019; 53: 1801913.

[23] Lau EM, Manes A, Celermajer DS and Galie N. Early detection of pulmonary vascular disease in pulmonary arterial hypertension: time to move forward. Eur Heart J 2011; 32: 2489-2498.

[24] Harel F, Fu Y, Nguyen QT, Letourneau M, Perrault LP, Caron A, Fournier A and Dupuis J. Use of adrenomedullin derivatives for molecular imaging of pulmonary circulation. J Nucl Med 2008; 49: 1869-1874.

[25] Tuder RM, Stacher E, Robinson J, Kumar R and Graham BB. Pathology of pulmonary hypertension. Clin Chest Med 2013; 34: 639-650.

[26] Dupuis J, Caron A and Ruel N. Biodistribution, plasma kinetics and quantification of single-pass pulmonary clearance of adrenomedullin. Clin Sci (Lond) 2005; 109: 97-102.

[27] Fu Y, Letourneau M, Nguyen QT, Chatenet D, Dupuis J and Fournier A. Characterization of the adrenomedullin receptor acting as the target of a new radiopharmaceutical biomolecule for lung imaging. Eur J Pharmacol 2009; 617: 118-123.

[28] Fu Y, Letourneau M, Chatenet D, Dupuis J and Fournier A. Characterization of iodinated adrenomedullin derivatives suitable for lung nuclear medicine. Nucl Med Biol 2011; 38: 867-874.

[29] Letourneau M, Nguyen QT, Harel F, Fournier A and Dupuis J. PulmoBind, an adrenomedullin-based molecular lung imaging tool. J Nucl Med 2013; 54: 1789-1796.

[30] Harel F, Langleben D, Provencher S, Fournier A, Finnerty V, Nguyen QT, Letourneau M, Levac X, Abikhzer G, Guimond J, Mansour A, Guertin MC and Dupuis J. Molecular imaging of the human pulmonary vascular endothelium in pulmonary hypertension: a phase II safety and proof of principle trial. Eur J Nucl Med Mol Imaging 2017; 44: 1136-1144.

[31] Levac X, Harel F, Finnerty V, Nguyen QT, Letourneau M, Marcil S, Fournier A and Dupuis J. Evaluation of pulmonary perfusion by SPECT imaging using an endothelial cell tracer in supine humans and dogs. EJNMMI Res 2016; 6: 43.

[32] Alonso Martinez LM, Harel F, Nguyen QT, Letourneau M, D'Oliviera-Sousa C, Meloche B, Finnerty V, Fournier A, Dupuis J and DaSilva JN. Al[(18)F]F-complexation of DFH17, a NOTA-conjugated adrenomedullin analog, for PET imaging of pulmonary circulation. Nucl Med Biol 2018; 67: 36-42.

[33] McBride WJ, Sharkey RM, Karacay H, D'Souza CA, Rossi EA, Laverman P, Chang CH, Boerman OC and Goldenberg DM. A novel method of 18F radiolabeling for PET. J Nucl Med 2009; 50: 991-998.

[34] Su AI, Cooke MP, Ching KA, Hakak Y, Walker JR, Wiltshire T, Orth AP, Vega RG, Sapinoso LM, Moqrich A, Patapoutian A, Hampton GM, Schultz PG and Hogenesch JB. Large-scale analysis of the human and mouse transcriptomes. Proc Natl Acad Sci U S A 2002; 99: 4465-4470.

[35] CFR 21 361.1. Available from: https://www.accessdata.fda.gov/scripts/cdrh/cfdocs/cfcfr/CFRSearch.cfm?FR=361.1.

[36] Hay DL, Walker CS and Poyner DR. Adrenomedullin and calcitonin gene-related peptide receptors in endocrine-related cancers: opportunities and challenges. Endocr Relat Cancer 2011; 18: C1-14.